

Synthesis and crystal structures of bis(dibenzyl dithiocarbamato)Cu(II) and Ag(I) complexes: Precursors for Cu_{1.8}S and Ag₂S nano-photocatalysts

Peter A. Ajibade*, Berlinda M. Sikakane, Nandipha L. Botha, Abimbola E. Oluwalana, Bernard Omondi

School of Chemistry and Physics, University of KwaZulu Natal, Private Bag X01, Scottsville, Pietermaritzburg, 3200, South Africa



ARTICLE INFO

Article history:

Received 16 May 2020

Received in revised form

18 June 2020

Accepted 27 June 2020

Available online 1 July 2020

Keywords:

Dibenzylidithiocarbamate
Crystal structures
Copper sulphide
Silver sulphide
Nano-photocatalyst.

ABSTRACT

We report the synthesis and crystal structures of bis(dibenzyl dithiocarbamato) copper(II) and silver(I) complexes and their use as precursors to prepare Cu_{1.8}S and Ag₂S nanoparticles. Single crystal analysis of bis(dibenzyl dithiocarbamato)Cu(II) complex consist of a monomeric entity where the two dibenzyl dithiocarbamate ligands form a distorted square planar geometry around the Cu(II) ion. The bis(dibenzyl dithiocarbamato)Ag(I) formed hexameric coordination complex consisting of two distorted hexagonal Ag₃S₃ rings. The complexes were thermolysed at 220 °C to prepare copper sulphide and silver sulphide nanoparticles. Powder X-ray diffraction (p-XRD) patterns of the copper sulphide nanoparticles were indexed to digenite Cu_{1.8}S, while silver sulphide nanoparticles were confirmed to be acanthinite Ag₂S. High-resolution transmission electron microscopy (HRTEM) images showed Ag₂S nanoparticles with particle size in the range 11.4–27.4 nm while Cu_{1.8}S nanoparticles are semi-spherical in shape with slightly agglomerated particles in the range 6.9–24.0 nm. The as-prepared nanoparticles were used as nano-photocatalysts for the degradation of methylene blue dye (MB) under UV light irradiation with degradation efficiency of 42.52% and 48.39% for Cu_{1.8}S and Ag₂S nanoparticles respectively.

© 2020 Elsevier B.V. All rights reserved.

1. Introduction

Interest in the synthesis of nanomaterials are due to their size-dependent properties and potential applications in medicine [1–3] and agriculture [4,5], among others. The chemical composition, size, shape and other physical properties of nanomaterials have been investigated to establish their potential applications [6–8]. The flexibility of metallic nanoparticles is ascribed to the synthetic techniques through which their sizes, shapes, compositions, as well as optical properties can be control [9,10]. Among metallic nanoparticles, great efforts have been dedicated to the synthesis and morphological control of metal chalcogenides nanoparticles of which copper sulphide and silver sulphide [11,12] are of paramount importance due to their stoichiometry and potential applications. Synthetic methods such as micro-emulsion [13], solvent-free [14], enzyme treatment [15], colloidal [16], substrate template [17] and single-source precursor [18] have been explored. Among these

synthetic routes, the thermolysis of single-source precursors are known to yield high quality nanoparticles due to the established metal-sulphur bond in the molecule through which the chemical composition and physical properties of the as-prepared metal sulphide can be control [19–23].

Copper sulphide (CuS) nanomaterials are being studied for applications in solar cells, optical filters, super ionic material, photovoltaic applications, and in combined photo acoustic imaging [24]. Silver sulphide (AgS) is the only semiconductor apart from mercury sulphide with three polymorphous phase modifications (α -Ag₂S, β -Ag₂S and γ -Ag₂S) [25]. The phase modification is attributed to transitions between superionic β -Ag₂S and semiconducting α -Ag₂S. This unique property makes them useful in infrared detectors in resistance-switches and non-volatile memory devices and recently quantum dots of silver sulphide are used as fluorescent labels [26]. In recent years, studies on photocatalytic activities of CuS and Ag₂S nanoparticles, are based on hybrids/composites [27,28]. Jiang et al. reported the photocatalytic degradation of methyl orange by Janus Ag–Ag₂S coupled with TiO₂ with efficiency of 80% after 50 min [29]. Yang et al. studied the photocatalytic activity of Ag₂S–Ag hybrid

* Corresponding author.

E-mail address: ajibadep@ukzn.ac.za (P.A. Ajibade).

nanotubes for degradation of methyl orange and reduction of Cr^{VI} under visible light irradiation and obtained a superior photocatalytic performance, which was ascribed to the enhanced charge transfer from the conduction band of Ag₂S to Ag in the hybrid [30]. Other studies have shown that the structural and optical properties of metal sulphide nanoparticles can be controlled through the precursor and synthetic routes [21,31–33]. In continuation of our effort to develop nanoparticles with controlled structural, morphological and optical properties using the single-source precursor approach, we present the syntheses and crystal structures of dibenzyl dithiocarbamate Cu(II) and Ag(I) complexes. The complexes were thermolyzed at 220 °C to prepare Cu_{1.8}S and Ag₂S nanoparticles. The structural and optical properties of the as-prepared nanoparticles were studied and their potential as nano-photocatalysts were evaluated using methylene blue photodegradation under visible light irradiation.

2. Experimental

2.1. Chemicals and characterization techniques

Dibenzyl amine, sodium hydroxide, carbon dioxide, silver(I) nitrate, copper(II) chloride, oleic acid, oleylamine, diethyl ether, chloroform, ethanol and toluene were purchased from Sigma-Aldrich and used as received without further purification. Electronic absorption and Fourier-Infrared (FTIR) analysis for the ligand and complexes were obtained using PerkinElmer lambda UV–Vis and Cary 630 FTIR (Agilent technologies) spectrometer. Different analytical techniques were used for the characterization of Cu_{1.8}S and Ag₂S nanoparticles. XRD patterns data for phase identification were collected on Bruker D8 Advance diffractometer with CuK α radiation ($\lambda = 1.5418 \text{ \AA}$). HRTEM images and selected area electron

diffraction (SAED) patterns were obtained using Japan electrical optical labs (JEOL) HRTEM-2100. ZEISS scanning electron microscope (SEM) equipped with an energy dispersive X-ray (EDX) spectrometer was used for surface morphology and elemental composition. Absorption and photoluminescence studies was done on PerkinElmer Lambda UV–Vis and PerkinElmer LS 45 fluorescence spectrometer respectively.

2.2. Synthesis of dibenzyl dithiocarbamate (dbdtc)

Dibenzyl dithiocarbamate (dbdtc) ligand was synthesized based on a modified literature method [22]. Cold dibenzyl amine (0.005 mol) was added to cold solution of sodium hydroxide (0.005 mol), followed by the dropwise addition of cold carbon disulphide (0.005 mol). The reaction was stirred for 2 h at about 4 °C. The white crystalline product was filtered, washed with diethyl ether and dried in a desiccator.

2.3. Synthesis of bis(dibenzyl dithiocarbamato)Cu(II) and Ag(I) complexes

The metal complexes were synthesized according to a modified literature method [22]. (0.005 mol; 0.8494 g) CuCl₂ or (0.01 mol; 0.4247 g) AgNO₃ was dissolved in 50 mL of water in a beaker. (0.01 mol; 2.95 g) dibenzyl dithiocarbamate (dbdtc) was dissolved in 50 mL in a separate beaker. Then the ligand solution was added into the respective metal salt solution and stirred for 4 h. The products were filtered, washed with water and dried under vacuum. Copper(II) dibenzyl dithiocarbamate ([Cu(dbdtc)₂]) was obtained as a brown solid while silver(I) dibenzyl dithiocarbamate ([Ag₃(dbdtc)₆]) was yellowish in colour.

Table 1
Crystal data and structure refinement for [Ag₃(dbdtc)₆] and [Cu(dbdtc)₂].

	[Ag ₃ (dbdtc) ₆]	[Cu(dbdtc) ₂]
Empirical formula	C ₉₂ H ₈₆ Ag ₆ Cl ₆ N ₆ S ₁₂	C ₃₀ H ₂₈ CuN ₂ S ₄
Formula weight	2520.30	608.32
Temperature	173(2) K	100(2) K
Wavelength	0.71073 Å	0.71073 Å
Crystal system	Triclinic	Triclinic
Space group	P $\bar{1}$	P $\bar{1}$
Unit cell dimensions (Å, °)	11.0126(6) 14.4254(8) 16.2955(10) 78.343(3) 73.321(2) 73.2140(10) 2354.0(2)	13.7098(9) 14.3201(10) 16.2979(11) 64.916(4) 72.302(3) 82.774(2) 2760.8(3)
V Å ³	2354.0(2)	2760.8(3)
Z	1	4
$\rho_{\text{calc}}/\text{mg m}^{-3}$	1.778	1.464
μ/mm^{-1}	1.709	1.117
F(000)	1256	1260
Crystal size (mm ³)	0.310 × 0.230 × 0.140	0.340 × 0.230 × 0.110
Theta range for data collection/°	1.316 to 26.500	1.437 to 27.597
Index ranges	-13 ≤ h ≤ 13 -182 ≤ k ≤ 18 -20 ≤ l ≤ 19	-17 ≤ h ≤ 17 -18 ≤ k ≤ 18 -20 ≤ l ≤ 21
Reflections collected	35157	39439
Independent reflections	9209 [R(int) = 0.0326] 94.7%	11444 [R(int) = 0.0485] 90.1%
Completeness to theta = 25.242°		
Absorption correction	Semi-empirical from equivalents	Semi-empirical from equivalents
Refinement method	Full-matrix least-squares on F ²	Full-matrix least-squares on F ²
Data/restraints/parameters	9209/0/550	11444/0/667
Goodness-of-fit on F ²	1.044	1.070
Final R indices [I > 2sigma(I)] R ₁ , wR ₂	0.0388, 0.0937	0.0446, 0.0914
R indices (all data) R ₁ , wR ₂	0.0502, 0.1006	0.0774, 0.1034
Extinction coefficient	n/a	n/a
Largest diff. peak and hole (e.Å ⁻³)	1.717 and -1.023	0.558 and -0.956

2.4. Synthesis of metal sulphide nanoparticles

The metal sulphide nanoparticles were synthesized using $[Ag_3(dbdtc)_6]$ and $[Cu(dbdtc)_2]$, 0.01 mol of the respective complex was added into an equimolar mixture of oleylamine and oleic acid in a three-necked flask. The reaction mixture was refluxed for 1 h at 220 °C under N₂ atmosphere and cooled to 70 °C. Cold ethanol was added into the solution, the resulting precipitate was collected by centrifugation.

2.5. Photocatalytic studies

Photocatalytic performance of the as-prepared nanoparticles was evaluated by measuring the degradation of methylene blue dye (10 mg/L) under visible light. In five 10 mL vials containing 5 mL of methylene blue solution, 3 mg of nanoparticles was added in each. The mixtures were sonicated for 5 min to form a homogenous suspension and stirred in a dark place magnetically for 30 min to attain adsorption-desorption equilibrium. The solutions were exposed to OSRAM VIALOX 70W incandescent mercury lamp (light source) 5 cm away at different time intervals (30, 60, 90 and 120 min). The samples were centrifuged to remove residual catalyst and dye degradation was analysed using UV–Vis spectrophotometry. Methylene blue dye absorbs at wavelength of 664 nm. The percentage (%) degradation was calculated using formula (1).

$$D (\%) = \frac{A_0 - A_t}{A_0} \times 100 \quad (1)$$

A plot of $\ln(A_0/A_t)$ vs irradiation time was obtained according to

a pseudo first-order kinetic model formula [34] (Eq (2)) which is expressed as follows:

$$\ln\left(\frac{A_0}{A_t}\right) = -k_t \quad (2)$$

where A_0 is the initial maximum absorbance at time 0, A_t is the maximum absorbance at time t and k is the rate constant.

2.6. X-ray crystallography

Crystals of $[Ag_3(dbdtc)_6]$ and $[Cu(dbdtc)_2]$ were obtained by slow evaporation of their respective chloroform solution. Crystal evaluation and data collection were performed on a Bruker Smart APEXII diffractometer with Mo K α radiation ($\lambda = 0.71073 \text{ \AA}$). The diffractometer to crystal distance was set at 4.00 cm. We obtained the initial cell-matrix from three series of scans at different starting angles. Each series consisted of 12 frames collected at intervals of 0.5° in a 6° range with an exposure time of 10 s per frame. Successful indexing of the reflections was done by an automated routine built in the APEXII program suite [35]. The final cell constants were calculated from a set of 6460 strong reflections from the actual data collection. Data collection method involved v scans of width 0.5°. The program SAINT plus [35] was used for data reduction and structure solved by direct methods using SHELXS [36] and refined using SHELXL [37]. All structures were checked for solvent-accessible cavities using PLATON [38] and the graphics were performed with the DIAMOND [39] visual crystal structure information system software as well as MERCURY. Non-H atoms were first refined isotropically and then by anisotropic refinement

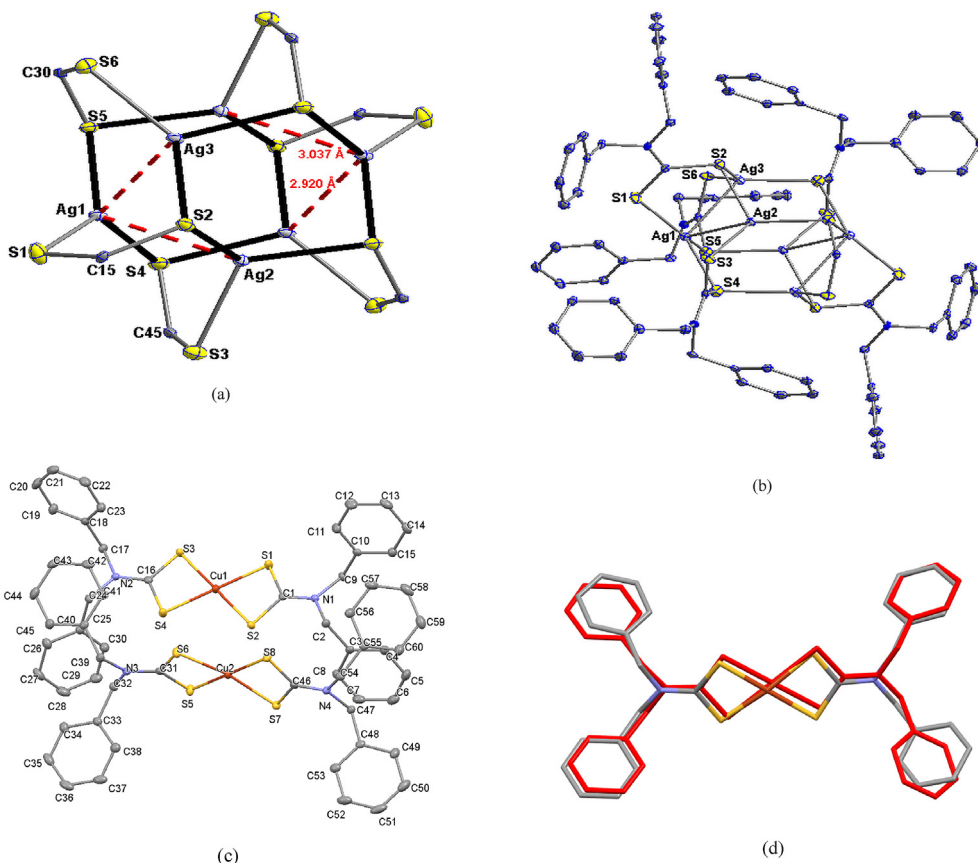


Fig. 1. (a) The hexagonal core consisting of Ag_3S_3 , (b) the molecular structure of $[Ag_3(dbdtc)_6]$, (c) the full molecular structure of $[Cu(dbdtc)_2]$, (d) an overlay of $[Cu(dbdtc)_2]$ molecules 1 and 2.

with full-matrix least-squares calculations based on F2 using SHELXS. We positioned all H atoms geometrically and allowed to ride on their respective parent atoms and refined isotropically. Absorption corrections were based on fitting a function to the empirical transmission surface as sampled by multiple equivalent measurements [39]. Crystal data and structure refinement information for $[\text{Ag}_3(\text{dbdtc})_6]$ and $[\text{Cu}(\text{dbdtc})_2]$ are summarized in Table 1.

3. Results and discussion

3.1. Molecular structures of Ag(I) and Cu(II) dibenzyl dithiocarbamate complexes

The molecular structure of $[\text{Ag}_3(\text{dbdtc})_6]$ is shown in Fig. 1a and b, selected bond distance (\AA) and bond angles ($^\circ$) are summarized in Table 2. $[\text{Ag}_3(\text{dbdtc})_6]$ crystallizes in the triclinic space group P\bar{1}. The complex has a core consisting of two distorted hexagonal Ag_3S_3 rings indicated by bold black bonds (see Fig. 1a) from which S–C–S–Ag moieties protrude to give a distorted hexagonal paddle wheel. Two Ag···Ag interactions (dashed red bonds) with distances of 2.9198(5) and 3.0374(5) \AA , which further supports the two Ag_3S_3 rings, as indicated in Fig. 1a. In this arrangement, two Ag atoms are coordinated by three S atoms from dibenzyl dithiocarbamate and an Ag···Ag interaction completing a distorted tetrahedral coordination geometry around the Ag atom. The third Ag centre in the asymmetric unit is coordinated by three S atoms and two Ag···Ag interactions resulting in a distorted five-coordinate Ag center [40].

In both cases the AgS_3 bite angle is essentially trigonal planar with S–Ag–S bond angles of 135.35(4), 129.72(4) and 91.95(3) for one Ag(I) centre, 117.67(4), 114.64(4) and 113.79(4) for the second Ag(I) centre and 137.30(4), 114.29(4) and 104.99(4) for the third Ag(I) centre, close to ideal trigonal planar arrangement. The Ag···Ag interactions point out of this plane and are not orthogonal. The other two Ag···Ag distances are long but are only interactions (3.3210(5) and 3.3465(5) \AA , which is shorter than the sum of two silver atoms Van der Waals (3.44 \AA) signifies the presence of Ag–Ag metallophilic bond [41].

The Ag–S distances range between 2.4421(11) to 2.5476(12) \AA and are comparable to those of related structures [40,42–44]. The C–S bond length of silver ranges between 1.710(2)–1.714(2) and these values are less than the typical C–S bond (1.8 \AA), hence showing a partial double bond character typical to dithiocarbamate complexes [45].

Copper(II) complexes of dithiocarbamate have three types of coordination geometry: they are five-coordinate dimers, infinite polymeric chain and square planar monomer [46]. Fig. 1c shows the molecular structure of $[\text{Cu}(\text{dbdtc})_2]$ with atom numbering scheme. $[\text{Cu}(\text{dbdtc})_2]$ has two non-symmetrically related molecules in the asymmetric unit. The Cu(II) center in the molecular structure of $[\text{Cu}(\text{dbdtc})_2]$ has a distorted square planar geometry. In this arrangement, the Cu(II) center accommodates two ligands each with Cu–S distances ranging from 2.2924(11) to 2.3231(8) \AA correlating with reported copper(II) dithiocarbamate complexes with four coordinate [46]. Fig. 1d shows an overlay of the two molecules of $[\text{Cu}(\text{dbdtc})_2]$, having a root mean square deviation of

0.5012 which is relatively high and is due to the difference in the orientation of the benzyl moieties of the molecules. The C–S bond length of copper complex ranges between 1.7178(13)–1.7272(13) \AA ; these values are less than the typical C–S bond (1.8 \AA), hence showing a partial double bond character typical to dithiocarbamate complexes [45]. The trans S4–Cu1–S1 and S2–Cu1–S3 angles are 179.26°(15) and 179.73°(16), respectively, which are slightly equal

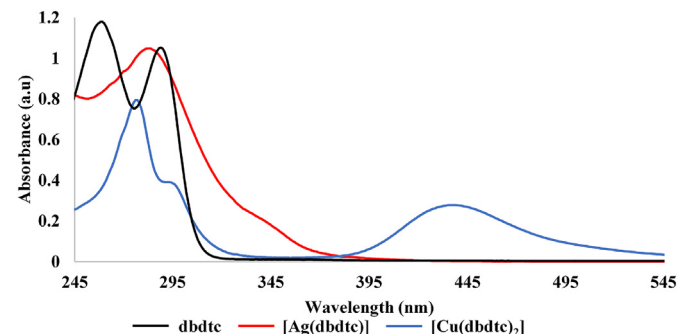


Fig. 2. Electronic spectra of the ligand and the metal complexes.

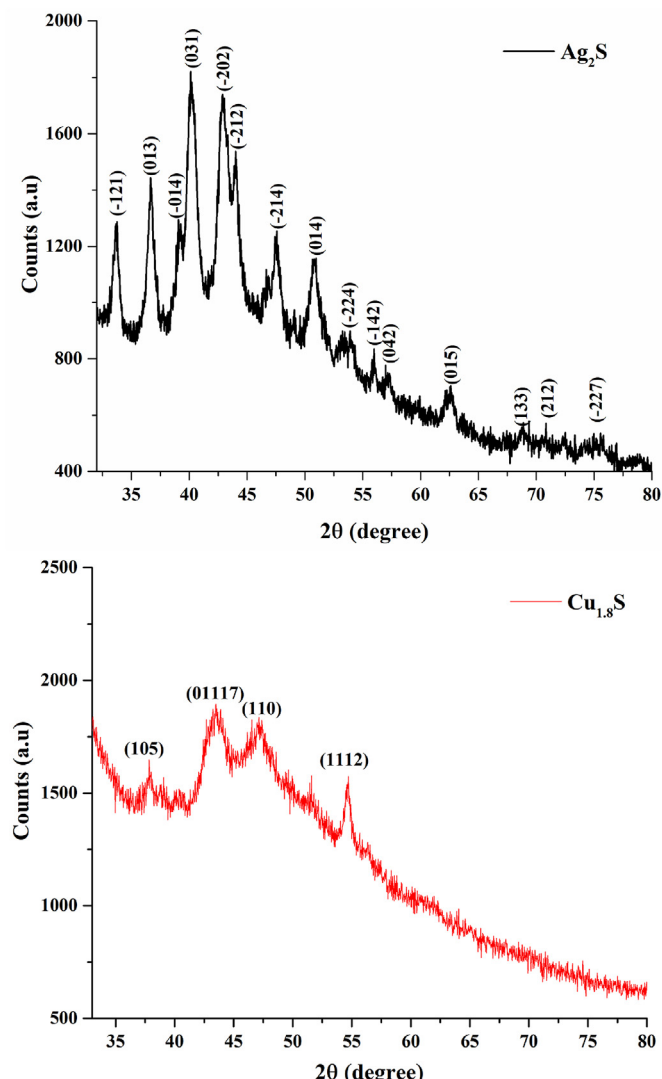


Fig. 3. Powder X-ray diffraction patterns of the metal sulphide nanoparticles.

Table 2
Important bond distances (\AA) and angles ($^\circ$).

Parameter	$[\text{Ag}_3(\text{dbdtc})_6]$	$[\text{Cu}(\text{dbdtc})_2]$
M–S ranges	2.4421(11) – 2.5476(12)	2.2924(9) – 2.3231(8)
M···M ranges	2.9198(5)–3.3465(5)	–
S–M–S ranges	91.95(3)–135.35(4)	77.48(3)–179.73(3)

and consistent with reported dithiocarbamate complexes with square planar environment [45,47].

3.2. Spectroscopic studies

The FTIR spectrum of the ligand shows two stretching vibrational bands at 972 cm^{-1} and 1032 cm^{-1} assigned to symmetric and asymmetric C–S vibrations, respectively [22]. These vibrations were replaced by one vibration in the complexes spectra at 985 cm^{-1} for $[\text{Ag}_3(\text{dbdtc})_6]$ and 976 cm^{-1} for $[\text{Cu}(\text{dbdtc})_2]$. This indicates that the ligand coordinated to the metal ions in symmetric bidentate chelating mode [45]. The C–N vibration was observed in the ligand at 1448 cm^{-1} which shifted to higher wavenumbers in the complexes at 1479 cm^{-1} and 1478 cm^{-1} for $[\text{Ag}_3(\text{dbdtc})_6]$ and $[\text{Cu}(\text{dbdtc})_2]$ respectively. This shift could be attributed to electron flow from the (N–CS₂) moiety to the metal centre, thereby increasing the C–N double bond character after coordination [46].

The overlay electronic spectra of the ligand and the complexes is displayed in Fig. 2. Three bands characterize the absorption of the

ligand (dbdtc) at 261 nm , 291 nm and a little shoulder at 367 nm which are attributed to ($\pi \rightarrow \pi^*$) from the N–C=S system, ($\pi \rightarrow \pi^*$) from the S–C=S group and ($n \rightarrow \pi^*$) due to lone pair of electron on sulphur atoms respectively [21]. The absorption of $[\text{Ag}_3(\text{dbdtc})_6]$ has only one band at 280 nm , which is assigned to $\pi \rightarrow \pi^*$ intra ligand charge-transfer transitions. $[\text{Cu}(\text{dbdtc})_2]$ showed three bands, the bands observed at 277 and 294 nm are assigned to $\pi \rightarrow \pi^*$ intraligand charge-transfer transitions. The third band is very broad and intense at 438 nm , which could be ascribed to $d_{xy} \rightarrow d_{xz}$ transitions of the Cu(II) ion in a square planar geometry. However, the band corresponding to $d_{xy} \rightarrow d_z^2$ transitions was not observed [48].

3.3. Structural studies of the nanoparticles

3.3.1. Powder X-ray diffraction of the nanoparticles

Fig. 3 show the powder X-ray diffraction patterns of the copper sulphide and silver sulphide nanoparticles. pXRD patterns of copper sulphide nanoparticles showed peaks at $2\theta = 38.09$, 43.75 , 47.40 and 54.90° , indexed to (105), (01117), (110) and (1112) planes

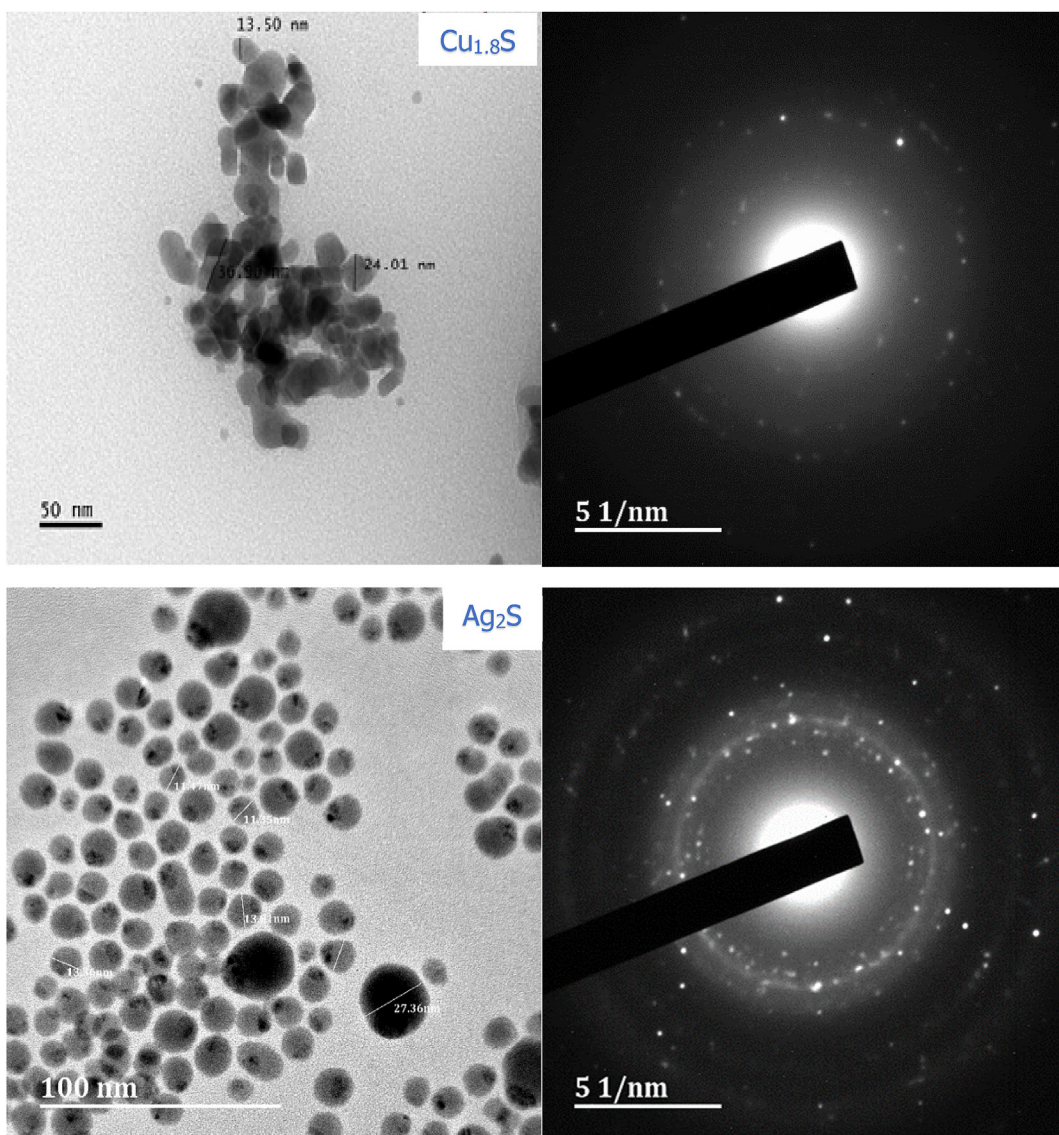


Fig. 4. HRTEM and SAED images of the metal sulphide nanoparticles.

of the digenite Cu_{1.8}S (JCPDS 95-005-3331) [49]. The p-XRD patterns of the silver sulphide nanoparticles showed diffraction peaks at $2\theta = 33.76, 36.67, 38.97, 40.12, 42.85, 44.02, 47.40, 50.79, 53.93, 55.01, 56.97, 68.88, 70.81$ and 76.59° corresponding to (-121), (013), (-014), (031), (-202), (-212), (-214), (014), (-224), (-142), (042), (015), (133), (-212) and (-227) miller indices respectively [50]. The patterns matched with the literature XRD patterns of acanthite Ag_{1.93}S crystalline phase [51]. The average particle size was calculated using the Debye-Scherrer equation (3) [52]:

$$D = \frac{0.9\lambda}{\beta \cos\theta} \quad (3)$$

where D is the average particle size, λ is the wavelength (1.5406 Å), β is the half-width peak at maximum, 0.9 is a constant and θ is the diffraction angle. The average particle size was 15.53 nm for Ag₂S and 26.42 nm for Cu_{1.8}S.

3.3.2. HRTEM and SEM images of the nanoparticles

The structural and morphological properties of the metal sulphide nanoparticles were studied using HRTEM and SEM. Fig. 4 shows monodispersed spherical Ag₂S nanoparticles with particle size in the range 11.4–27.4 nm. For Cu_{1.8}S, the nanoparticles are agglomerated semi-spherically shaped particles with size in the

range 6.9–24.0 nm. This might be due to the high themolysis temperature (220 °C), which favours the Oswald ripening process [53] in Cu_{1.8}S. The thermolysis of the Ag(I) complex precursor favours the formation of mono-dispersed spherically shaped Ag₂S nanoparticles [54]. Also, from Fig. 4, the Ag₂S selected area electron diffraction (SAED) patterns showed distinct rings confirming the crystallinity of the particles. However, SAED patterns of the Cu_{1.8}S showed two circular rings patterns that are blurred by amorphous layers deposited on the surface ascribed to the capping agent. The results obtained confirm that the capping agent (oleylamine) and the reducing agent (oleic acid) used worked well with [Ag(dbdtc)] than [Cu(dbdtc)₂] as single-source precursor [55].

Silver sulphide shows clustered fibre layers in the SEM micrograph while copper sulphide nanoparticles shows plain or smooth surface morphology. The EDX spectra confirmed the presence of the respective metals and sulphur in the particles. The spectra also showed the carbon and oxygen peaks which are attributed to the capping agent coordinated to the surface of the particles.

3.3.3. Optical studies of metal sulphide nanoparticles

Absorption and emission spectra of the as-prepared nanoparticles are presented in Fig. 5 were obtained using Ultraviolet–Visible absorption analysis and photoluminescence, The absorption band edge of Ag₂S appeared at 286 nm, while that of

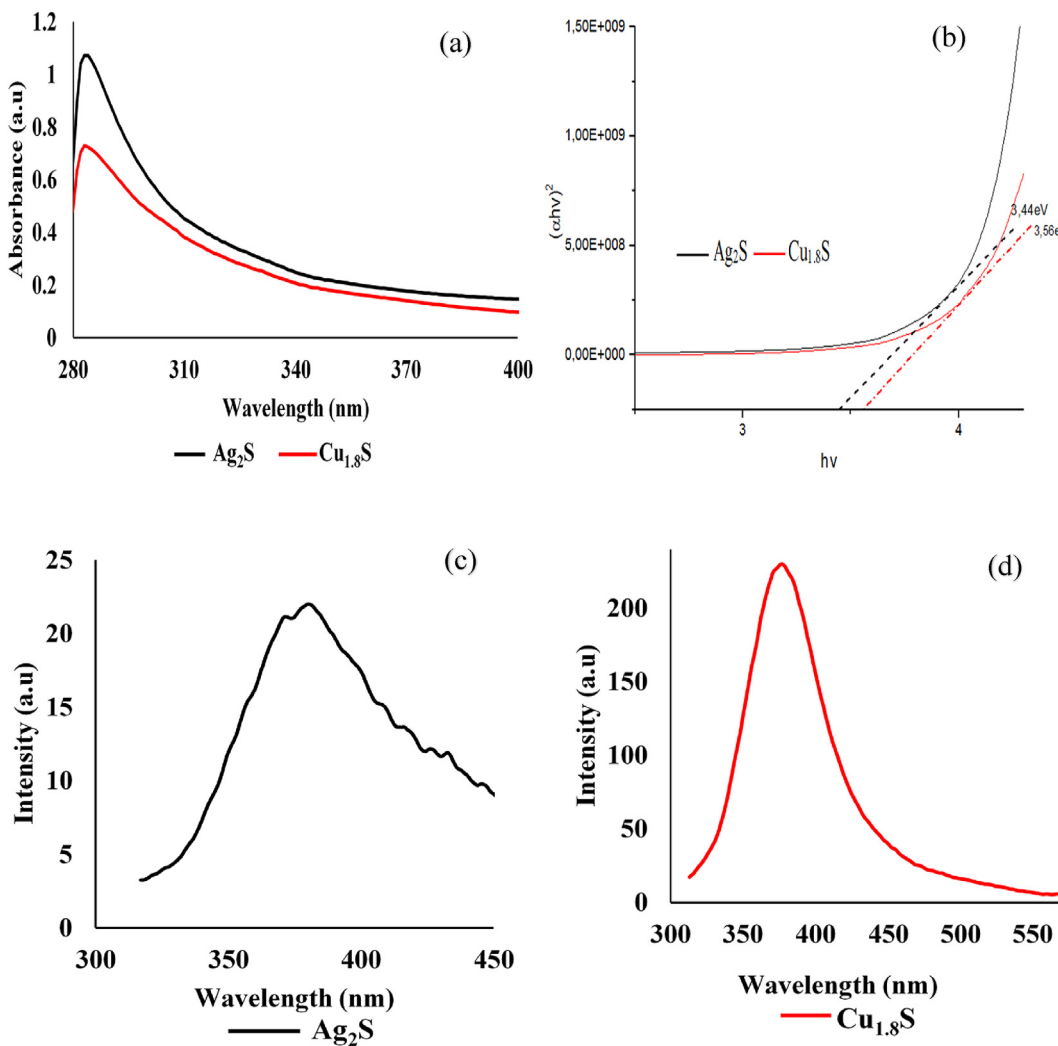


Fig. 5. Absorption (a), Tauc's plot (b) and emission spectra (c,d) of the metal sulphide nanoparticles.

$\text{Cu}_{1.8}\text{S}$ appeared at 284 nm. This indicates that the nanoparticles will absorb ultraviolet radiation and excites its atoms to upper levels [56]. The bandgap energies of the as-prepared nanoparticles obtained from the Tauc plots (Fig. 5b) are 3.44 eV and 3.56 eV for Ag_2S and $\text{Cu}_{1.8}\text{S}$ nanoparticles, respectively. These values are greater than the bandgap energies of bulk Ag_2S (0.9–1.11 eV) and $\text{Cu}_{1.8}\text{S}$ (1.21 eV) [25,57].

The results revealed that the energy bandgap of the as-prepared nanoparticles is blue-shifted, showing the effect of quantum confinement which is due to the decrease in the size of the nanoparticles [58]. The emission spectra of the nanoparticles (Fig. 5c) showed emission peaks observed at 382 nm and 379 nm for Ag_2S and $\text{Cu}_{1.8}\text{S}$ respectively, which is attributed to trapped electron-hole recombination on the surface of the nanoparticle [22]. The emission peaks are red shifted in comparison to Ag_2S and $\text{Cu}_{1.8}\text{S}$ absorption band edges at 286 nm and 284 nm. In addition, Ag_2S has a lower emission intensity compared to $\text{Cu}_{1.8}\text{S}$, which means it has a low electron-hole pair recombination rate which will help in photocatalytic efficiency [59].

3.4. Photocatalytic studies

The time-dependent photocatalytic degradation graphs of methylene blue (MB) dye in the presence of $\text{Cu}_{1.8}\text{S}$ and Ag_2S are

presented in Fig. 6a–b, which shows that the intensity of absorbance peak at 664 nm for MB dye decreases with an increase in irradiation time. $\text{Cu}_{1.8}\text{S}$ and Ag_2S nanoparticles were able to degrade 42.52% and 48.39% of MB dye after 120 min, respectively. Ag_2S shows higher photocatalytic activity compared to $\text{Cu}_{1.8}\text{S}$ nanoparticles which may be attributed to the better separation of the electron-hole pairs, while the less activity of the $\text{Cu}_{1.8}\text{S}$ nanoparticles can be attributed to rapid recombination of electron-hole pairs [59]. Most Ag_2S nanoparticles used for photocatalysis are coupled with other metal sulphides or metal oxides nanoparticles. To the best of our knowledge, the only Ag_2S nanoparticles used for photocatalysis with high efficiency have porous worm-like morphology and low bandgap energy (~1.01–1.03 eV) [60]. Also, the reduced efficiency of $\text{Cu}_{1.8}\text{S}$ nanoparticles might be due to its smooth surface morphology and surface interaction with the dye molecule as Cu_2S nanoparticles reported with high efficiency has flower-like morphology [61–63].

Langmuir-Hinshelwood kinetic model [64] was used to describe the photocatalytic degradation of methylene blue dye by the nanoparticles. Fig. 6d shows a plot of $\ln(A_0/A_t)$ vs irradiation time. Rate constants of 0.0051 min^{-1} and 0.0065 min^{-1} were obtained for $\text{Cu}_{1.8}\text{S}$ and Ag_2S respectively which indicate pseudo-first-order kinetics. The rate constant obtained further supports that Ag_2S nanoparticles exhibit more photocatalytic activity when compared

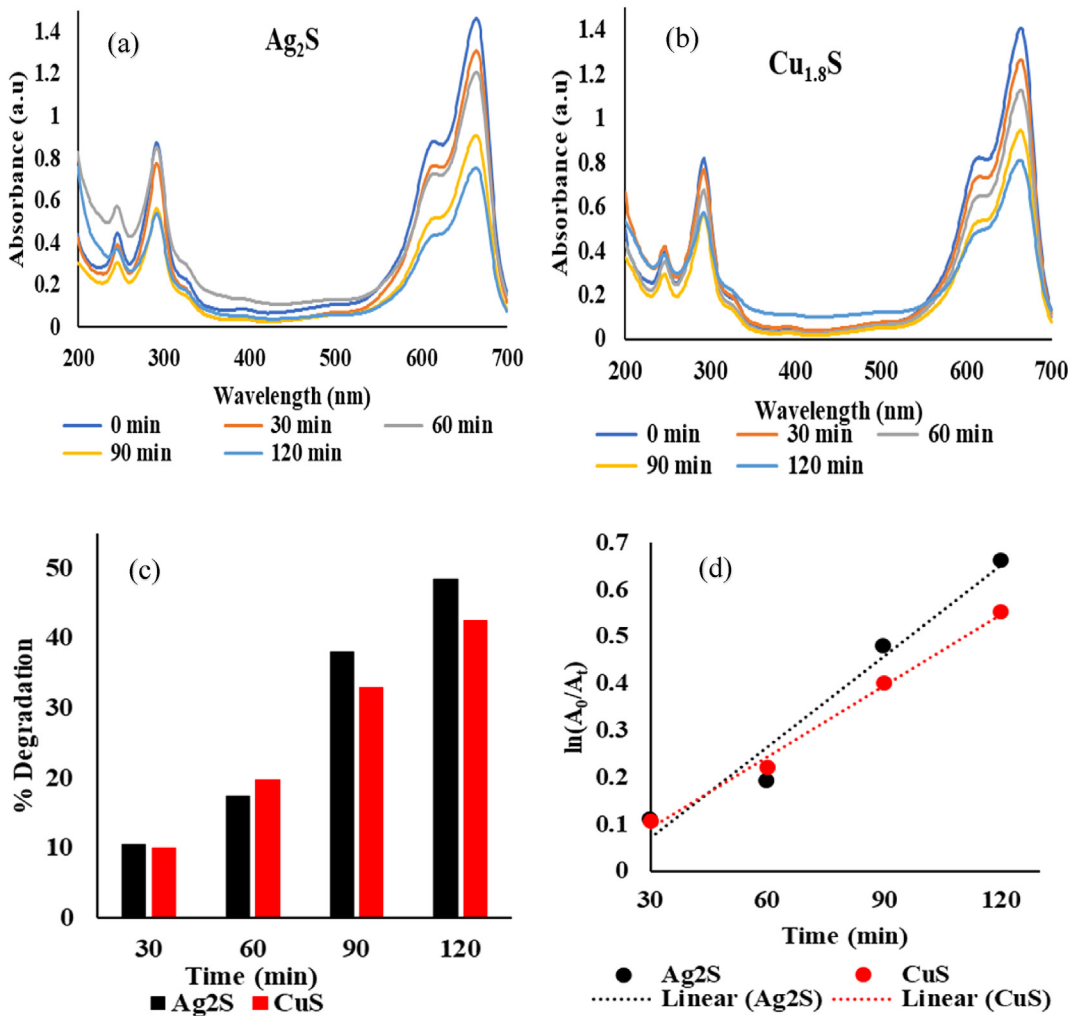


Fig. 6. MB UV–Vis absorption degradation spectra (a,b), degradation efficiency bar chart (c) kinetic plot of $\ln(A_0/A_t)$ versus irradiation time (d) in the presence of Ag_2S and $\text{Cu}_{1.8}\text{S}$ nanoparticles.

to Cu_{1.8}S nanoparticles since the rate constant of Ag₂S is higher than that of Cu_{1.8}S nanoparticles. The linear relationship between the ln(A₀/A_t) and irradiation time shows a good correlation of pseudo-first-order kinetics.

4. Conclusion

Dibenzyl dithiocarbamato copper(II) and silver(I) complexes were synthesized and characterized using single crystal X-ray crystallography. Molecular structure of the Ag(I) complex reveals hexameric configuration in which three Ag atoms are bonded to six molecules of didenzyldithiocarbamato ligands leading to the formation of two distorted hexagonal Ag₃S₃ rings. The Cu(II) dibenzyl dithiocarbamate complex consists of a monomeric complex with two dibenzyl dithiocarbamate bounded to the Cu(II) in a distorted square planar geometry. The complexes were thermolyzed at 220 °C to prepared digenite copper sulphide (Cu_{1.8}S) and acathinite silver sulphide (Ag₂S) nanoparticles. HRTEM images showed copper sulphide with mixture of semi spherical particles that are slightly agglomerated in the range 6.9–24.0 nm while silver sulphide nanoparticles are monodispersed spherically shaped nanoparticles with particle size in the range 11.4–27.4 nm. The photocatalytic degradation of methylene blue dye by the Ag₂S and Cu_{1.8}S were evaluated under UV irradiation. The degradation efficiency of 42.52% and 48.39% were obtained for Cu_{1.8}S and Ag₂S nanoparticles respectively. Ag₂S was found to be more efficient, which is an indication that it may find potential application as nano-photocatalyst.

Supplementary data

CCDC 1864305 and 1864306 contain the supplementary crystallographic data for this paper. These data can be obtained free of charge at www.ccdc.cam.ac.uk/conts/retrieving.html or from the Cambridge crystallographic data centre, 12 Union Road, Cambridge, CB2 1EZ, UK; fax: (+44)-1223-336-033 or email: deposit@ccdc.cam.ac.uk.

Author statement

This research work was conducted as part of the postgraduate training of BMS, NLB and AEO under the mentorship of **PAA**, **BMS**, **NLB** and **AEO** each did part of the experiments, data analyses and draft manuscript while BO wrote the description of the crystal structures. **PAA** was responsible for conceptualization, funding acquisition, project administration, supervision, writing of draft, review and final editing.

Declaration of competing interest

The authors declare that they have no known competing financial interests or personal relationships that could have appeared to influence the work reported in this paper.

Acknowledgements

The authors gratefully acknowledged NRF financial support.

References

- [1] M. De, P.S. Ghosh, V.M. Rotello, Applications of nanoparticles in biology, *Adv. Mater.* 20 (2008) 4225–4241.
- [2] I.S. Chekman, Z.R. Ulberg, N.O. Gorchakova, T.Y. Nebesna, T.G. Gruzina, A.O. Priskokha, A.M. Doroshenko, P.V. Simonov, The prospects of medical application of metal-based nanoparticles and nanomaterials, *Lik Sprava* 1 (2011) 3–21.
- [3] K. McNamara, S.A. M Tofail, Nanoparticles in biomedical applications, *Adv. Phys.* 2 (2017) 54–88.
- [4] S. Singh, B.K. Singh, S.M. Yadav, A.K. Gupta, Applications of nanotechnology in agricultural and their role in disease management, *Res. J. Nanosci. Nanotechnol.* 5 (2015) 1–5.
- [5] X. Zhang, Z. Xu, M. Wu, X. Qian, D. Lin, H. Zhang, J. Tang, T. Zeng, W. Yao, J. Filser, L. Li, Potential environmental risks of nanopesticides: application of Cu(OH)₂ nanopesticides to soil mitigates the degradation of neonicotinoid thiacloprid, *Environ. Int.* 129 (2019) 42–50.
- [6] K.W. Powers, M. Palazuelos, B.M. Moudgil, S.M. Roberts, Characterization of the size, shape, and state of dispersion of nanoparticles for toxicological studies, *Nanotoxicology* 1 (2007) 42–51.
- [7] X. Zhang, Z. Xu, A. Wimmer, H. Zhang, J. Wang, Q. Bao, Z. Gu, M. Zhu, L. Zeng, L. Li, Mechanism for sulfidation of silver nanoparticles by copper sulfide in water under aerobic conditions, *Environ. Sci. Nano.* 5 (2018) 2819–2829.
- [8] E. Shi, Z. Xu, X. Zhang, X. Yang, Q. Liu, H. Zhang, A. Wimmer, L. Li, Re-evaluation of stability and toxicity of silver sulfide nanoparticle in environmental water: oxidative dissolution by manganese oxide, *Environ. Pollut.* 243 (2018) 1242–1251.
- [9] S.C. Subbaiai, Physical and chemical nature of nanoparticles, *Plant Nanotech* 2 (2016) 15–27.
- [10] Y. Zhang, Y. Zhao, Z. Xu, H. Su, X. Bian, S. Zhang, X. Dong, L. Zeng, T. Zeng, M. Feng, L. Li, Carbon quantum dots implanted CdS nanosheets: efficient visible-light-driven photocatalytic reduction of Cr(VI) under saline conditions, *Appl. Catal., B* 262 (2020) 118306.
- [11] M.T. Ramesan, P. Jayakrishnan, T. Anilkumar, G. Mathew, Influence of copper sulphide nanoparticles on the structural, mechanical and dielectric properties of poly (vinyl alcohol)/poly (vinyl pyrrolidone) blend nanocomposites, *J. Mater. Sci. Mater. Electron.* 29 (2018) 1992–2000.
- [12] A.B. Patil, B.M. Banhave, Shape selectivity using ionic liquids for the preparation of silver and silver sulphide nanomaterials, *Phys. Chem. Chem. Phys.* 16 (2014) 3027–3035.
- [13] J.N. Solanki, R. Sengupta, Z.V.P. Murthy, Synthesis of copper sulphide and copper nanoparticles with microemulsion method, *Solid State Sci.* 12 (2010) 1560–1566.
- [14] K.M. Bhunia, E. Abou-Hamad, D.H. Anjum, A. Gurinov, K. Takanabe, Solvent-free synthesis of quaternary metal sulfide nanoparticles derived from thiourea, *Part. Part. Syst. Char.* 35 (2018) 1700183.
- [15] Y.Y. Kim, D. Walsh, Metal sulfide nanoparticles synthesized via enzyme treatment of biopolymer stabilized nanosuspensions, *Nanoscale* 2 (2010) 240–247.
- [16] S.I. Sadovnikov, Y.V. Kuznetsova, A.A. Rempel, Ag₂S silver sulfide nanoparticles colloidal solutions: synthesis and properties, *Nano-Struct. Nano-Object.* 7 (2016) 81–91.
- [17] R. Chen, N. Nuhfer, L. Moussa, P.M. Whitmore, Silver sulfide nanoparticle assembly obtained by reacting an assembled silver nanoparticle template with hydrogen sulfide gas, *Nanotechnology* 19 (2008) 455604.
- [18] Z. Zhang, W.P. Lim, C.T. Wong, H. Xu, F. Yin, W.S. Chin, From metal thio-benzoates to metal sulfide nanocrystals: an experimental and theoretical investigation, *Nanomaterials* 2 (2012) 113–133.
- [19] S. Shen, Y. Zhang, L. Peng, B. Xu, Y. Du, M. Deng, H. Xu, Q. Wang, Generalized synthesis of metal sulfide nanocrystals from single-source precursors: size, shape and chemical composition control and their properties, *CrystEngComm* 13 (2011) 4572–4579.
- [20] I. Jen-La Plante, T.W. Zeid, P. Yang, T. Mokari, Synthesis of metal sulfide nanomaterials via thermal decomposition of single-source precursors, *J. Mater. Chem.* 20 (2010) 6612–6617.
- [21] N.L. Botha, P.A. Ajibade, Effect of temperature on crystallite sizes of copper sulfide nanocrystals prepared from copper(II) dithiocarbamate single source precursor, *Mater. Sci. Semicond. Process.* 43 (2016) 149–154.
- [22] A.M. Paca, P.A. Ajibade, Synthesis and structural studies of iron sulphide nanocomposites from iron(III) dithiocarbamate single source precursors, *Mater. Chem. Phys.* 202 (2017) 143–150.
- [23] Y. Ma, H. Wan, Y. Ye, L. Chen, H. Li, H. Zhou, J. Chen, In-situ synthesis of size-tunable silver sulfide nanoparticles to improve tribological properties of the polytetrafluoroethylene-based nanocomposite lubricating coatings, *Tribol. Int.* 148 (2020) 106324.
- [24] P. Roy, S.K. Srivastava, Nanostructured copper sulfides: synthesis, properties and applications, *CrystEngComm* 17 (2015) 7801–7815.
- [25] S.I. Sadovnikov, A.I. Gusev, Recent progress in nanostructured silver sulfide: from synthesis and nonstoichiometry to properties, *J. Mater. Chem. A* 5 (2017) 17676–17704.
- [26] S.I. Sadovnikov, A.I. Gusev, A.A. Rempel, Nanocrystalline silver sulfide Ag₂S, *Rev. Adv. Mater. Sci.* 41 (2015) 7–19.
- [27] S.L. Lee, C.J. Chang, Recent Progress on metal sulfide composite nanomaterials for photocatalytic hydrogen production, *Catalysts* 9 (2019) 457.
- [28] E. Shi, Z. Xu, W. Wang, Y. Xu, Y. Zhang, X. Yang, Q. Liu, T. Zeng, S. Song, Y. Jiang, L. Li, Ag₂S-doped core-shell nanostructures of Fe₃O₄@Ag₃PO₄ ultrathin film: major role of hole in rapid degradation of pollutants under visible light irradiation, *Chem. Eng. J.* 366 (2019) 123–132.
- [29] F. Jiang, Q. Tian, M. Tang, Z. Chen, J. Yang, J. Hu, One-pot synthesis of large-scaled Janus Ag–Ag₂S nanoparticles and their photocatalytic properties, *CrystEngComm* 13 (2011) 7189–7193.
- [30] W. Yang, L. Zhang, H. Yu, Y.Y. Zhong, H.B. Wu, X.W.D. Lou, Microwave-assisted synthesis of porous Ag₂S–Ag hybrid nanotubes with high visible-light

- photocatalytic activity, *Angew. Chem. Int. Ed.* 51 (2012) 11501–11504.
- [31] L.L. Mphahlele, P.A. Ajibade, Synthesis and crystal structure of bis(morpholino dithiocarbamato)Cd(II) complex and its use as precursor for CdS quantum dots using different capping agents, *J. Sulfur Chem.* 40 (2019) 648–663.
- [32] A.M. Paca, P.A. Ajibade, Synthesis, optical, and structural studies of iron sulphide nanoparticles and iron sulphide hydroxyethyl cellulose nanocomposites from bis-(dithiocarbamato)iron(II) single-source precursors, *Nanomaterials* 8 (2018) 187.
- [33] A.E. Oluwalana, P.A. Ajibade, Synthesis and crystal structures of Pb(II) dithiocarbamates complexes: precursors for PbS nanophotocatalyst, *J. Sulfur Chem.* 41 (2020) 182–199.
- [34] S. Chakrabarti, B. Dutta, Photocatalytic degradation of model textile dyes in wastewater using ZnO as semiconductor catalyst, *J. Hazard Mater.* 112 (2004) 269–278.
- [35] A.P.E.X. Bruker, Saint and SADABS, Bruker AXS Inc., Madison, Wisconsin, USA, 2009.
- [36] G.M. Sheldrick, A short history of SHELX, *Acta Crystallogr. A: Found Crystallogr.* 64 (2008) 112–122.
- [37] C.B. Hubschle, G.M. Sheldrick, B. Dittrich SheIxl, A Qt graphical user interface for SHELXL. Journal of applied crystallography, *J. Appl. Crystallogr.* 44 (2011) 1281–1284.
- [38] A.L. Spek, Single-crystal structure validation with the program PLATON, *J. Appl. Crystallogr.* 36 (2003) 7–13.
- [39] T.A. Jones, A graphics model building and refinement system for macromolecules, *J. Appl. Crystallogr.* 11 (1978) 268–272.
- [40] Q. Zhang, R. Cao, M. Hong, W. Su, H. Liu, Polynuclear silver compound formed from aggregation of Se²⁻ and Ag(I)-thiolate complex. Synthesis, structure and spectroscopic characterization of Ag₁₁(μ₅-Se)(μ₄-Et₂NCS₂)₃(μ₃-Et₂NCS₂)₆, *Inorg. Chim. Acta* 277 (1998) 171–176.
- [41] M.A. Ehsan, H. Khaledi, A.A. Tahir, H.N. Ming, K.U. Wijayantha, M. Mazhar, Synthesis and characterization of silver diethyldithiocarbamate cluster for the deposition of acanthite (Ag₂S) thin films for photoelectrochemical applications, *Thin Solid Films* 536 (2013) 124–129.
- [42] Z. Huang, X. Lei, M. Hong, Liu, Crystal and molecular structure of a polysilver cluster molecule with an unusual bridging sulfur atom, Ag₁₁S(Et₂dte)₉, *Inorg. Chem.* 31 (1992) 2990–2991.
- [43] W. Su, M. Hong, F. Jiang, H. Liu, Z. Zhou, D. Wu, T.C.W. Mak, A cleavage of the SC bond in 2-aminothiophenol: synthesis and crystal structure of [Ag₁₁(μ₅-S)(μ₄-S₂CNET₂)₆(μ₃-S₂CNET₂)₃], *Polyhedron* 15 (1996) 4047–4051.
- [44] X. Yin, M.B. Xie, W.G. Zhang, J. Fan, Poly [(μ₃-N, N-dibenzylidithiocarbamato-κ⁴S,S':S') silver(I)], *Acta Crystallogr. E* 63 (2007) m2273-m2273.
- [45] P.A. Ajibade, A.A. Fatokun, F.P. Andrew, Synthesis, characterization and anti-cancer studies of Mn(II), Cu(II), Zn(II) and Pt(II) dithiocarbamate complexes-crystal structures of the Cu(II) and Pt(II) complexes, *Inorg. Chim. Acta* (2020) 119431.
- [46] G. Gurumoorthy, S. Thirumaran, S. Ciattini, Synthesis and characterization of copper(II) dithiocarbamate complexes involving pyrrole and ferrocenyl moieties and their utility for sensing anions and preparation of copper sulfide and copper–iron sulfide nanoparticles, *Appl. Organomet. Chem.* 32 (2018) e4363.
- [47] Y.W. Cui, L. Wu, W. Yue, F. Lian, J. Qu, Two polypyridyl-chelating nickel(II) and copper(II) complexes: synthesis, structural characterization and in vitro anticancer activity in osteogenic sarcoma, *J. Mol. Struct.* 1191 (2019) 145–151.
- [48] S.R. Trifunović, Z. Marković, D. Sladić, D.M. Andjelković, K.K. Sabo, T.J. Minić, Popović, The synthesis and characterization of nickel(II) and copper(II) complexes with the polydentate dialkyl dithiocarbamic acid ligand 3-dithiocarboxy-3-aza-5-aminopentanoate, *J. Serb. Chem. Soc.* 67 (2002) 115–122.
- [49] P. Kumar, M. Gusain, R. Nagarajan, Synthesis of Cu1.8S and CuS from copper-thiourea containing precursors; anionic (Cl⁻, NO₃⁻, SO₄²⁻) influence on the product stoichiometry, *Inorg. Chem.* (2011) 3065–3070.
- [50] S.I. Sadovnikov, A.I. Gusev, A.A. Rempel, Nonstoichiometry of nanocrystalline monoclinic silver sulphide, *Phys. Chem. Chem. Phys.* 17 (2015) 12466–12471.
- [51] A.I. Gusev, S.I. Sadovnikov, Acanthite–argentite transformation in nanocrystalline silver sulfide and the Ag₂S/Ag nanoheterostructure, *Semiconductors* 50 (2016) 682–687.
- [52] A. Shawky, S.M. El-Sheikh, A. Gaber, S.I. El-Hout, I.M. El-Sherbiny, A.I. Ahmed, Urchin-like CuS nanostructures: simple synthesis and structural optimization with enhanced photocatalytic activity under direct sunlight, *Appl. Nanosci.* (2020) 1–12.
- [53] S. Jain, N. Nagar, V. Devra, Synthesis and characterization of highly efficient copper nanoparticles and their catalytic application in oxidative kinetic study, *Adv. Appl. Sci. Res.* 6 (2015) 171–180.
- [54] C. Zhang, S. Zhang, L. Yu, Z. Zhang, P. Zhang, Z. Wu, Size-controlled synthesis of monodisperse Ag₂S nanoparticles by a solventless thermolytic method, *Mater. Lett.* 85 (2012) 77–80.
- [55] L. Xu, X. Zhang, Y. Shen, Y. Ding, L. Wang, Y. Sheng, Durable superhydrophobic cotton textiles with ultraviolet-blocking property and photocatalysis based on flower-like copper sulfide, *Ind. Eng. Chem. Res.* 57 (2018) 6714–6725.
- [56] S. Riyaz, A. Parveen, A. Azam, Microstructural and optical properties of CuS nanoparticles prepared by sol–gel route, *Perspect. Sci.* 8 (2016) 632–635.
- [57] Y. Wu, C. Wadia, W. Ma, B. Sadler, A.P. Alivisatos, Synthesis and photovoltaic application of copper(I) sulfide nanocrystals, *Nano Lett.* 8 (2008) 2551–2555.
- [58] L. Yanhong, W. Dejun, Z. Qidong, Y. Min, Z. Qinglin, A study of quantum confinement properties of photogenerated charges in ZnO nanoparticles by surface photovoltage spectroscopy, *J. Phys. Chem.* 108 (2004) 3202–3206.
- [59] G. Murugadoss, R. Jayavel, M.R. Kumar, R. Thangamuthu, Synthesis, optical, photocatalytic, and electrochemical studies on Ag₂S/ZnS and ZnS/Ag₂S nanocomposites, *Appl. Nanosci.* 6 (2016) 503–510.
- [60] B.M. Alshehri, M. Shkir, T.M. Bawazeer, S. AlFaify, M.S. Hamdy, A rapid microwave synthesis of Ag₂S nanoparticles and their photocatalytic performance under UV and visible light illumination for water treatment applications, *Physica E Low Dimens. Syst. Nanostruct.* (2020) 114060.
- [61] B. Srinivas, B.G. Kumar, K. Muralidharan, Stabilizer free copper sulphide nanostructures for rapid photocatalytic decomposition of rhodamine B, *J. Mol. Catal. Chem.* 410 (2015) 8–18.
- [62] U. Shamraiz, A. Badshah, R.A. Hussain, M.A. Nadeem, S. Saba, Surfactant free fabrication of copper sulphide (CuS–Cu₂S) nanoparticles from single source precursor for photocatalytic applications, *J. Saudi Chem. Soc.* 21 (2017) 390–398.
- [63] M. Baláž, E. Dutková, Z. Bujňáková, E. Tóthová, N.G. Kostova, Y. Karakirova, J. Briančin, M. Kaňuchová, Mechanochemistry of copper sulfides: characterization, surface oxidation and photocatalytic activity, *J. Alloys Compd.* 746 (2018) 576–582.
- [64] A. Dasari, V. Guttena, Sunlight-driven competent photocatalytic degradation of crystal violet using sonochemically produced GO capped Ag₂S nanocomposites, *Mater. Today Commun.* 19 (2019) 157–169.